Available online at www.sciencedirect.com
ScienceDirect
Journal of Hazardous Materials 155 (2008) 601–609
Journal of Hazardous Materials
www.elsevier.com/locate/jhazmat

Removal of basic dye from aqueous medium using a novel agricultural waste material: Pumpkin seed hull

B.H. Hameed [a,*], M.I. El-Khaiary [b]

[a] *School of Chemical Engineering, Engineering Campus, Universiti Sains Malaysia, 14300 Nibong Tebal, Penang, Malaysia*
[b] *Chemical Engineering Department, Faculty of Engineering, Alexandria University, El-Hadara, Alexandria 21544, Egypt*

Received 24 October 2007; received in revised form 25 November 2007; accepted 26 November 2007
Available online 4 December 2007

Abstract

In this work, pumpkin seed hull (PSH), an agricultural solid waste, is proposed as a novel material for the removal of methylene blue (MB) from aqueous solutions. The effects of the initial concentration, agitation time and solution pH were studied in batch experiments at 30 °C. The equilibrium process was described well by the multilayer adsorption isotherm. The adsorption kinetics can be predicted by the pseudo-first-order and the modified pseudo-first-order models. The mechanism of adsorption was also studied. It was found that for a short time period the rate of adsorption is controlled by film diffusion. However, at longer adsorption times, pore-diffusion controls the rate of adsorption. Pore diffusion takes place in two distinct regimes, corresponding to diffusion in macro- and mesopores. The results demonstrate that the PSH is very effective in the removal of MB from aqueous solutions.

Keywords: Adsorption isotherm; Kinetic; Methylene blue; Pumpkin seed hull; Pore diffusion

1. Introduction

The major industrial wastewater polluters in Malaysia are food and beverage processors, electric and electronics industries, chemical-based industries, textiles industries, and rubber and palm oil industries. The textile industry contributes about 22% of the total volume of industrial wastewater generated in the country [1]. Dye-containing wastewaters are well-known pollutants of receiving bodies in industrial areas. Much focus and attention have been placed upon the removal of dyes from waste streams due to the adverse effects of dyes on the environment [2]. There are many structural varieties of dyes, such as acidic, basic, disperse, azo, diazo, anthroquinone based and metal complex dyes. Basic dyes are widely used in acrylic, nylon, silk, and wool dyeing. Most of these dyes are toxic, mutagenic and carcinogenic. Therefore, their removal from industrial effluents before discharging into the environment is extremely important.

Activated carbon has been widely investigated for the adsorption of basic dyes [3–6], but its high cost limits its commercial application. Recently, various low-cost adsorbents derived from agricultural waste, industrial by-products or natural materials, have been investigated intensively for dye removal from aqueous solutions. Many researchers have investigated the use of cheap and efficient alternative substitutes to remove dyes from wastewater. Some of these alternative adsorbents are palm ash and chitosan/oil palm ash [7,8], shale oil ash [9], *Posidonia oceanica* (L.) fibres [10], water-hyacinth [11], pomelo (*Citrus grandis*) peel [12], de-oiled soya and bottom ash, [13], sunflower seed shells and mandarin peelings [14], sawdust [15], wheat bran [16], guava leaf powder [17] and almond shells [18].

Agro wastes are currently receiving attention as raw materials for water pollution control because of their availability and low-cost. In this context, we are investigating the potential of pumpkin seed hulls (PSH), an agricultural solid waste, as an alternative low-cost dye adsorbent. According to the authors' knowledge, no attempt has been made until now to use pumpkin seed hull for removal of basic dyes from aqueous solutions. Pumpkin, *Cucurbita pepo* L., is a herbaceous, monoecious, annual plant of the Cucurbitaceae family [19,20]. It is one of the most highly demanded vegetables in Asia and the Pacific region. The larger kinds acquire a weight of 18–36 kg but smaller varieties are in vogue for garden culture. The hull of a pumpkin

* Corresponding author. Tel.: +60 4 5996422.
E-mail address: chbassim@eng.usm.my (B.H. Hameed).

0304-3894/$ – see front matter © 2007 Elsevier B.V. All rights reserved.
doi:10.1016/j.jhazmat.2007.11.102

seed is a naturally occurring fibrous coat that serves to protect the inner seed. This hull is considered a beneficial source of fiber. To make better use of this cheap and abundant agricultural waste, it is proposed to use it as an adsorbent to remove basic dye from aqueous solutions. Thus, the purpose of the present work was to test the possibility of using the pumpkin seed hull for the removal of methylene blue from aqueous solutions. The second objective was to investigate the ability of three isotherms models; namely the Langmuir, the Freundlich and the multilayer adsorption isotherms, to model the equilibrium adsorption data. Finally, kinetic studies have been conducted to determine the rate of MB adsorption on PSH and to study the mechanism of the process.

2. Materials and methods

2.1. Adsorbate

The basic dye used in this study is methylene blue (MB) purchased from Sigma–Aldrich. The MB was chosen in this study because of its known strong adsorption onto solids. The maximum absorption wavelength of this dye is 668 nm. The structure of MB is shown in Scheme 1.

2.2. Adsorbent

Raw pumpkin seeds obtained from a local market were dehulled manually in the laboratory. The collected hulls were washed several times with boiled water and finally with deionized water to remove any adhering dirt. It was then oven dried at 70 °C for 24 h to constant weight. The dried sample was crushed, sieved to a particle size range of 0.5–1 mm, and stored in plastic bottle for further use. No other chemical or physical treatments were used prior to adsorption experiments.

2.3. Scanning electron microscopy and Fourier transform infra red study

Scanning electron microscopy (SEM) analysis was carried out on the PSH to study its surface texture before and after adsorption. Fourier Transform Infrared (FTIR) analysis was applied on the PSH to determine the surface functional groups, by using FTIR spectroscope (FTIR-2000, PerkinElmer), where the spectra were recorded from 4000 to 400 cm^{-1}.

2.4. Adsorption studies

Adsorption experiments were carried out by adding a fixed amount of adsorbent (0.30 g) into 250-mL Erlenmeyer flasks containing 200 mL of different initial concentrations (25, 50, 100, 150, 200, 250 and 300 mg/L) of dye solution and pH 7. The flasks were agitated in an isothermal shaker at 120 rpm and 30 °C for 110 min until equilibrium was reached. Aqueous samples were taken from the solutions and the concentrations were analyzed. At time $t = 0$ and at equilibrium, the dye concentrations were measured by a double beam UV/vis spectrophotometer (Shimadzu, Model UV 1601, Japan) at 668 nm. The amount of equilibrium adsorption, q_e (mg/g), was calculated by

$$q = \frac{(C_0 - C_e)V}{W} \quad (1)$$

where C_0 and C_e (mg/L) are the liquid-phase concentrations of dye at initial and equilibrium, respectively. V is the volume of the solution (L) and W is the mass of dry sorbent used (g).

The effect of initial solution pH was determined by agitating 0.30 g of PSH and 200 mL of dye solution of initial basic dye concentration 25 mg/L in a water-bath shaker (30 °C) at different solution pH values ranging from 2 to 11. Agitation was provided for 110 min contact time which is sufficient to reach equilibrium with a constant agitation speed of 120 rpm. The pH was adjusted by adding a few drops of diluted 1.0N NaOH or 1.0N HCl before each experiment. The pH was measured by using a pH meter (Ecoscan, EUTECH Instruments, Singapore).

Kinetic experiments were identical to those of equilibrium tests. The aqueous samples were taken at preset time intervals and the concentrations of MB were similarly measured. All the kinetic experiments were carried out at pH 7. The amount of sorption at time t, q (mg/g), was calculated by:

$$q = \frac{(C_0 - C_t)V}{W} \quad (2)$$

where C_t (mg/L) is the liquid-phase concentrations of dye at any time.

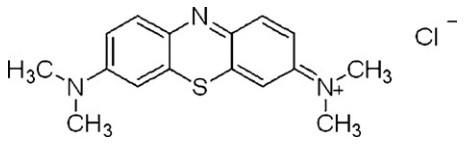

Scheme 1. The chemical structure of MB.

3. Results and discussion

3.1. SEM and FTIR of PSH

Fig. 1 shows the SEM micrographs of PSH samples before and after dye adsorption. It is clear that PSH has considerable numbers of heterogeneous pores where there is a good possibility for dye to be trapped and adsorbed. The surface of dye-loaded adsorbent, however, clearly shows that the surface of PSH is covered with a layer of dye.

The FTIR spectrum of PSH (Figure is not shown) shows distinct peaks at 3922.60–3445.63 cm^{-1} (OH stretch), 2928.47 cm^{-1} (CH stretch shift), 2361.19, 2341.47, 2290.88 cm^{-1} (NH stretch), 1747.36 cm^{-1} (C=O stretch disappeared), 1655.14, 1651.05 cm^{-1} (NH_2 deformation), 1498.02 cm^{-1} (phenyl), 1458.13 cm^{-1} (CH_2 deformation), 1020.42 cm^{-1} (C–O–C stretch), 670.37, 661.89 cm^{-1} (C–O–H twist). It is clear that the adsorbent displays a number of absorption peaks, reflecting the complex nature of the adsorbent. The FTIR spectrum of dye adsorbed PSH shows (Figure is not shown) peaks at 3787.78, 3571.19, 3435.68 cm^{-1} (OH stretch), 2929.70 cm^{-1} (CH stretch), 2349.45 cm^{-1} (NH stretch), 1649.43 cm^{-1} (NH_2 deformation), 1458.08 cm^{-1}

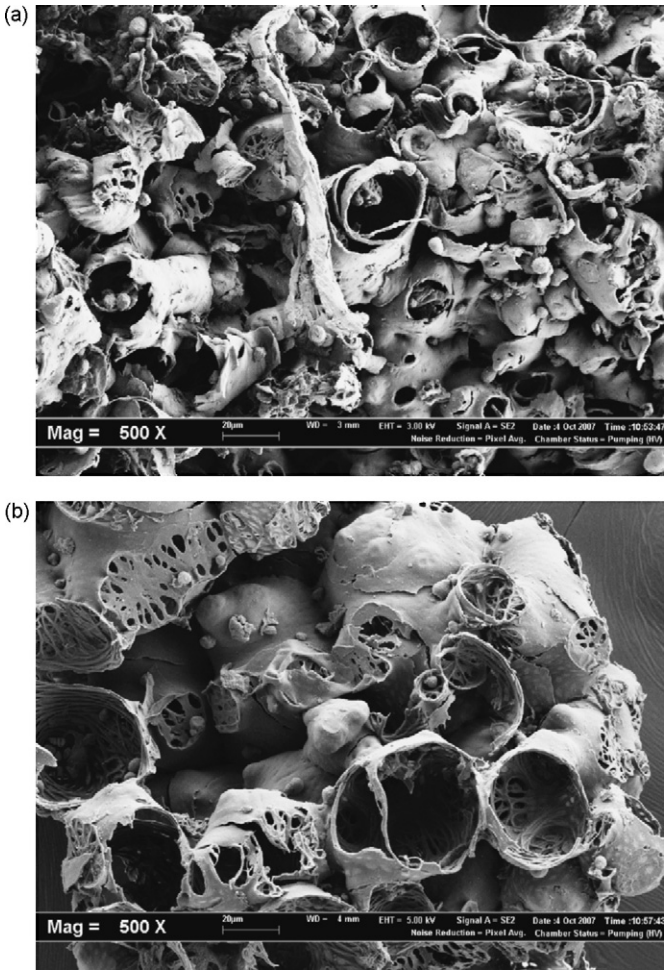

Fig. 1. SEM micrograph of PSH particle (magnification: 500): (a) before dye sorption and (b) with dye adsorbed.

(CH_2 deformation), 1053.14, 1032.23 cm^{-1} (C–O stretch), and 527.57 cm^{-1} (C–Cl stretch). The results indicate that some peaks were shifted or disappeared, and that new peaks are also detected. These changes observed in the spectrum indicate the possible involvement of those functional groups on the surface of the PSH in biosorption process.

3.2. Effect of initial concentration and agitation time on dye adsorption

Adsorption experiments were conducted to study the effect of the initial concentration of MB in the solutions on the rate of dye adsorption on PSH. The experiments were carried out at a fixed adsorbent dose (0.30 g) and at different initial dye concentrations of malachite green (25, 50, 100, 150, 200 and 300 mg/L) for different time intervals (5, 10, 15, 20, 30, 40, 50,70, 90 and 110 min) at 30 °C as shown in Fig. 2. It was observed that dye uptake is rapid for the first 10 min and thereafter it proceeds at a slower rate and finally attains saturation. This maybe explained by a rapid adsorption on the outer surface, followed by slower adsorption inside the pores. As the initial MB concentration increases from 25 to 300 mg/L the equilibrium removal of MB decreases from 60.76 to 31.63%. This may

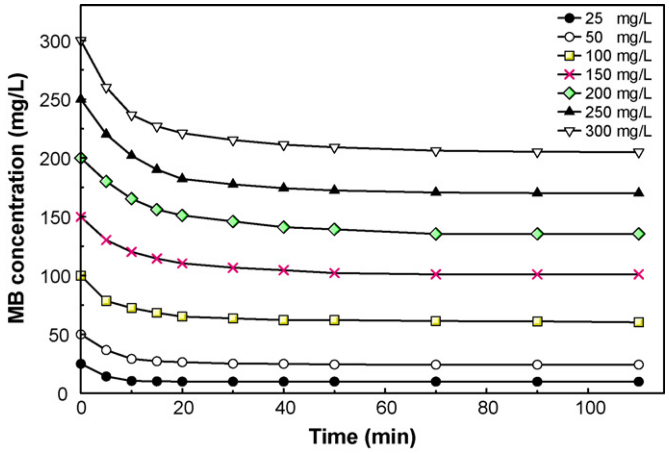

Fig. 2. Effect of initial concentration and contact time on MB adsorption (adsorbent dose = 0.30 g; Temperature = 30 °C).

be due to the fact that at lower concentrations almost all the dye molecules were adsorbed very quickly on the outer surface, but further increases in initial dye concentrations led to fast saturation of PSH surface, and thus most of the dye adsorption took place slowly inside the pores. It is also shown in Fig. 2 that for the initial MB concentrations of 25 and 50 mg/L, equilibrium is reached in about 20 min. For MB solutions with initial concentrations of 100–300 mg/l, equilibrium time of 40–70 min was required. However, the experimental data were measured at 110 min to make sure that full equilibrium was attained. Data on the adsorption kinetics of MB by various adsorbent have shown a similar range of adsorption rates. For example, Bulut and Aydın [21] have studied methylene blue adsorption on wheat shells and reported around 135 min equilibrium adsorption time. For adsorption of methylene blue on fallen phoenix tree's leaves, equilibrium was reached in 150 min [22].

3.3. Effect of solution pH on dye adsorption

The effect of pH was studied between 2 and 11 and the results at initial concentration of 25 mg/L. Fig. 3 shows the effect of initial solution pH on the amount of dye adsorbed at equilibrium conditions (mg/g) for the adsorption of MB on PSH. It can be seen from Fig. 3 that removal of MB was high at pH (6–9) and above pH 9 no further increase takes place. The amount of dye adsorbed increased from 9.67 to 15.33 mg/g for an increase in pH from 6 to 11. At lower pH, the surface charge may get positively

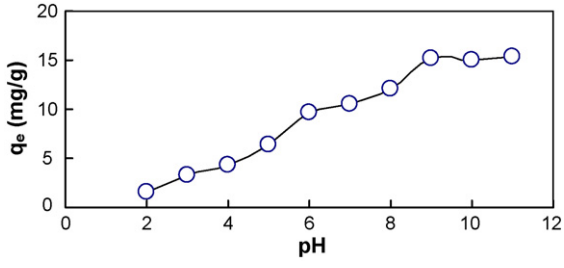

Fig. 3. Effect of pH on equilibrium uptake of MB (W = 0.30 g; V = 0.20 L; C_0 = 25 mg/L).

charged, thus making (H^+) ions compete effectively with dye cations causing a decrease in the amount of dye adsorbed [10]. Also lower adsorption of MB at acidic pH is probably due to the presence of excess H^+ ions competing with the cation groups on the dye for adsorption sites of PSH. When the pH increased, adsorbed MB also increases. This can be explained with the electrostatic interaction of MB with negatively charged surface of PSH [23].

3.4. Equilibrium isotherms

Three isotherms were tested for their ability to describe the experimental results, namely the Freundlich isotherm, the Langmuir isotherm, and the multilayer adsorption isotherm. The thermodynamic assumptions of the best fitting isotherm provide insight into both the surface properties and the mechanism of adsorption.

The Freundlich isotherm is used for non-ideal adsorption on heterogeneous surfaces. The heterogeneity is caused by the presence of different functional groups on the surface, and also by various mechanisms of adsorbent–adsorbate interactions. The Freundlich isotherm is represented by the following empirical equation [24]:(3)$q_e = K_F C_e^{1/n}$where K_F is the Freundlich adsorption constant and $1/n$ is a measure of the adsorption intensity.

The derivation of the Langmuir isotherm is based on the assumption of ideal monolayer adsorption on a homogenous surface. It is expressed by [25]:

$$q_e = \frac{q_m K_a C_e}{1 + K_a C_e} \tag{4}$$

where C_e is the equilibrium concentration (mg/L), q_e the amount of dye adsorbed at equilibrium (mg/g), q_m is q_e for complete monolayer adsorption capacity (mg/g), and K_a is the equilibrium adsorption constant (L/mg).

The adsorption in a multilayer equilibrium type is formulated as

$$\begin{aligned}
&\text{First layer adsorption :} && \underline{S} + M \Leftrightarrow \underline{S} - M; && K_1\\
&\text{Second layer adsorption :} && \underline{S} - M + M \Leftrightarrow \underline{S} - M_2; && K_2\\
&\text{Third layer adsorption :} && \underline{S} - M_2 + M \Leftrightarrow \underline{S} - M_3; && K_3\\
&. && . &&\\
&. && . &&\\
&n\text{th layer adsorption :} && \underline{S} - M_{n-1} + M \Leftrightarrow \underline{S} - M_n; && K_n
\end{aligned} \tag{5}$$

where $\underline{S}$ represents the available surface sites (mg/g), M the equilibrium concentration of MB, $\underline{S} - M_n$ the surface complex (mg/g), and K_n (L/mg) is the equilibrium adsorption constant of the nth layer. It is expected that the adsorption affinity of the first layer (K_1) will be much greater than the subsequent layers (K_2, K_3, …, and K_n) because dye adsorption within the multilayer results from the attachment of the dye to the surface and to the subsequent layers. Therefore, it follows that the adsorption affinity for subsequent layers would be the same, i.e. $K_2 = K_3 = \ldots = K_n$. The total multilayer adsorption capacity (Γ, mg/g) can be expressed by the following Eq. [26]:

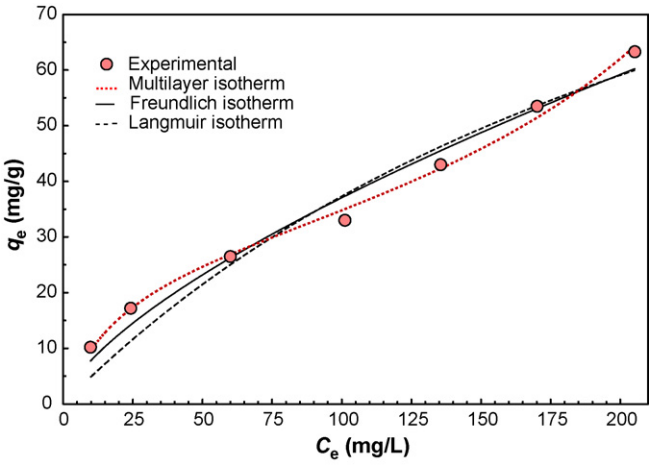

Fig. 4. Isotherm plots for MB adsorption on PSH at 30 °C.

$$\Gamma = \frac{[(\Gamma_m K_1 C_e)(1 - (K_2 C_e)^n)]}{((1 - K_2 C_e)[1 + (K_1 - K_2) C_e])} \tag{6}$$

where Γ_m is the monolayer adsorption capacity (mg/g) and C_e is the equilibrium MB concentration (mg/L). In the case of multilayer adsorption, the amount of MB adsorbed in a subsequent layer must be smaller than that in the previous layer. Therefore, the term $(K_2 C_e)^n \approx 0$, and Eq. (6) can be simplified to:

$$\Gamma = \frac{\Gamma_m K_1 C_e}{((1 - K_2 C_e)[1 + (K_1 - K_2) C_e])} \tag{7}$$

It can be seen that for ideal monolayer adsorption K_2 will have a value of zero, and Eq. (7) will be reduced to the monolayer Langmuir isotherm of Eq. (4).

Fig. 4 shows the fitted equilibrium data to Freundlich, Langmuir, and the multilayer adsorption (MLA) expressions. The fitting results, i.e. isotherm parameters and the coefficients of determination, R^2, are shown in Table 1. It can be seen in Fig. 4 that the MLA curve fits the data better than Freundlich and Langmuir models, this is also confirmed by the high value of R^2 in case of MLA (0.9990) compared to Freundlich (0.9928) and Langmuir (0.9575). This indicates that the adsorption of MB on PSH takes place as a multilayer adsorption on a surface that

Table 1
Isotherm constants for MB adsorption on PSH at 30 °C

Langmuir isotherm	
q_m (mg/g)	141.92
K_a (L/mg)	0.00357
R^2	0.9507
Freundlich isotherm	
K_f	1.648
n	1.479
R^2	0.9775
Multilayer adsorption model	
Γm (mg/g)	29.07
K_1 (L/mg)	0.0467
K_2 (L/mg)	0.00276
R^2	0.9953

is homogenous in adsorption affinity. The inflection point in the multilayer isotherm is seen at about $C_e \approx 71$ mg/L, which means that the second layer of adsorption begins when $C_e \approx 71$ mg/L and the corresponding value of q_e (from Table 1) is 29.07 mg/g.

3.5. Specific surface area determination

Specific surface area (SSA) is the accessible area of adsorbent surface per unit mass of material. The phase surrounding the adsorbent can modify the surface area; and therefore, each method used for measuring the surface area has its shortcomings and uncertainties. The interference by the surrounding phase is especially problematic for the BET N_2 adsorption/desorption isotherm method because the entire surface is modified by the application of vacuum before N_2 adsorption. As an alternative to the BET method, the adsorption of dyes from aqueous solution has been used to determine the SSA of many substances such as layered silicate [27], sludge ash [28], and cotton [29]. Assuming that the PSH surface is homogenous and completely covered by dye molecules, the SSA (m^2/g) of PSH can then be related to the first layer adsorption density (Γ_m) as described in Eq. (8):

$$\mathrm{SSA} = \Gamma_m N A \tag{8}$$

where N is the Avogadro's number (6.023×10^{23} molecules/mol) and A is the apparent surface area occupied by one MB molecule. Studies have shown that MB molecules are adsorbed in a flat orientation on fibrous cellulosic materials, so that the occupied surface area of one molecule of MB is196 $Å^2$ [30]. The SSA of PSH calculated from Eq. (8) is 91.79 m^2/g.

3.6. Adsorption kinetics

The two most widely used equations for adsorption kinetics are Lagergren's pseudo-first order model (Eq. (9)) [31], and Ho's pseudo-second-order model (Eq. (10)) [32],

$$q = q_e(1 - e^{-k_1 t}) \tag{9}$$

$$q = \frac{(q_e^2 k_2 t)}{(1 + q_e k_2 t)} \tag{10}$$

where q_e is the amount of adsorbate adsorbed at equilibrium (mg/g), q is the amount of adsorbate adsorbed at time t (mg/g), k_1 is the rate constant of pseudo-first order adsorption (min^{-1}), k_2 is the rate constant of pseudo-second-order adsorption (g/mg min).

Recently Yang and Al-Duri [33] proposed a modified pseudo-first-order model that successfully described the adsorption of

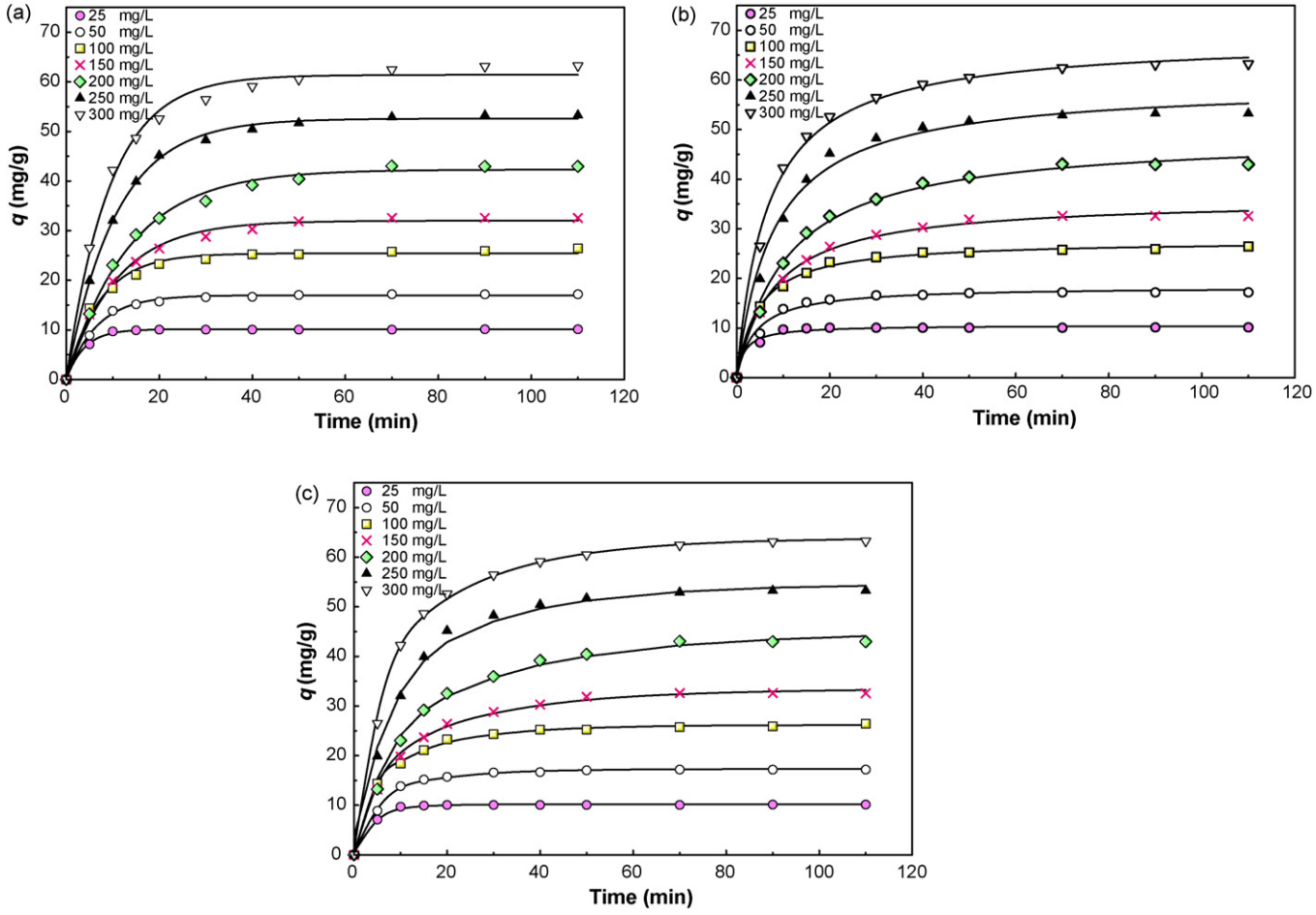

Fig. 5. (a) The fitting of pseudo-first-order model for MB on PSH for different initial concentrations at 30 °C. (b) The fitting of pseudo-second-order model for MB on PSH for different initial concentrations at 30 °C. (c) The fitting of the modified pseudo-first-order model for MB on PSH for different initial concentrations at 30 °C.

reactive dyes on activated carbon. In this model, which has no theoretical derivation, the pseudo first-order equation is modified through its rate constant by replacing k_1 by K_1, where $k_1 = K_1(q_e/q)$ which gives the rate equation:

$$q = q_e(1 - e^{-((q/q_e)+K_1 t)}) \quad (11)$$

The fittings of the experimental kinetic results to Eqs. (9)–(10) were done by nonlinear regression. Eq. (11) cannot be fitted directly because q is present in both sides of the equation, so it was fitted to the data by nonlinear minimization of the sum of squared deviations from zero of the formula:

$$q - q_e(1 - e^{-((q/q_e)+K_1 t)}) \quad (12)$$

The fitting results are shown in Fig. 5a–c, and the values of the estimated parameters are presented in Table 2. It was found that the modified pseudo-first-order model gives good fitting to our experimental data, almost just as good as the normal pseudo-first-order model, but not better. Both models have almost similar R^2 values, and both models predict q_e with similar accuracy. The normal performance of the modified pseudo-first-order model in our study in spite of its superiority in the study of Yang and Al-Duri [33] can be attributed to their use of the following linearized form of Eq. (11):

$$\frac{q_t}{q_e + \ln(q_e - q_t) = \ln(q_e) - K_1 t} \quad (13)$$

and plotting $(q_t/q_e + \ln(q_e - q_t))$ against t, thus obtain a straight line whose slope equals K_1. The transformations applied to linearize the equation distorted the error distribution of the data and changed the relative weights of data points [34], leading to exaggerated correlation coefficients.

On comparing the values of the coefficient of determination, R^2, it is not possible to decide which model has the best agreement with the experimental data. Although the pseudo second-order model has relatively low R^2 values (0.9833, 0.9873) for initial MB concentrations 25 and 50 mg/L, the fits are good at higher concentrations and R^2 values are in the range 0.9905–0.9977. On the other hand, the pseudo-first-order model has a moderate fit for initial MB concentration 100 mg/L ($R^2 = 0.9892$), but for all other concentrations the R^2 values are in the range 0.9939–0.9987. The modified pseudo-first order model also has good fit for all initial concentration with R^2 values are in the range 0.9930–0.9984. Therefore, it is concluded that at low concentrations of MB the pseudo-second-order model is not suitable, while at concentrations higher than 50 mg/L, the three models can be used for modeling and prediction of the experimental kinetic data of MB adsorption on PSH.

By inspecting the values of k_1, K_1, and k_2 in Table 2, it is found that the values of the rate constants decrease with increasing the initial concentration of MB from 25 to 200 mg/L. A larger rate constant implies that it will take shorter time for the adsorption system to reach the same fractional uptake. Therefore, the trend that k_1, K_1, and k_2 decrease with increasing C_0 in the range 25–200 mg/L only reveals the fact that it is faster for an adsorption system with a lower initial concentration to reach a specific fractional uptake. However, on increasing C_0 above 200 mg/L, it is seen that k_1, K_1, and k_2 show a slight increase. This suggests that increasing C_0 has two opposing effects: a high concentration means more competition between MB molecules for adsorption sites, but a high concentration leads also to enhancement in mass transfer. It seems that up to 200 mg/L the effect of less competition is dominant, but at higher concentrations the increase in mass transfer becomes high enough to increase the rate of adsorption. This conclusion is corroborated by the results of mass transfer study (Section 3.7).

The initial rates of adsorption (at time = zero) were calculated from the pseudo first and second order models from the equations:

$$h_{0,1} = k_1 q_e, \quad h_{0,1m} = K_1 q_e \quad (14)$$

$$h_{0,2} = k_2 q_e^2 \quad (15)$$

and the results are plotted in Fig. 6. The major trend seen in the figure is an increase in the initial rate of adsorption with increasing the initial concentration; this is explained by increasing the driving force for adsorption at higher concentrations. It is also noticed in the figure that for $C_0 = 100$ mg/L the initial rate of adsorption is higher than the general trend of the curve; this concentration also corresponds to the beginning of the second adsorption layer. It is not clear whether the high value of h_0 is related to the beginning of multilayer adsorption or is a result of experimental error in determining the concentration of MB at the early stages of the adsorption period.

3.7. Mechanism of adsorption

For the process design and control of adsorption systems, it is important to understand the dynamic behavior of the system. At

Table 2
Kinetic models parameters for the adsorption of MB on PSH at 30 °C and different initial MG concentrations (C_0: mg/L; q_e: mg/g; k_1: 1/min; k_2: g/mg min, K_1: 1/min)

C_0	q_{exp}	Pseudo-first-order			Pseudo-second-order			Modified pseudo-first-order		
		q_e	k_1	R^2	q_e	k_2	R^2	q_e	K_1	R^2
25	10.13	10.12	0.257	0.9980	10.54	0.0555	0.9833	10.16	0.140	0.9930
50	17.18	16.98	0.153	0.9972	18.36	0.0136	0.9873	17.29	0.0693	0.9970
100	26.45	25.43	0.137	0.9892	27.68	0.00784	0.9977	26.18	0.0554	0.9984
150	32.59	32.00	0.0926	0.9945	36.01	0.00350	0.9970	33.48	0.0348	0.9967
200	42.97	42.31	0.0740	0.9959	48.87	0.00188	0.9948	45.15	0.0256	0.9950
250	53.24	52.60	0.0938	0.9987	59.25	0.00213	0.9905	54.60	0.0372	0.9931
300	63.25	61.40	0.107	0.9939	68.40	0.00221	0.9962	63.87	0.0412	0.9971

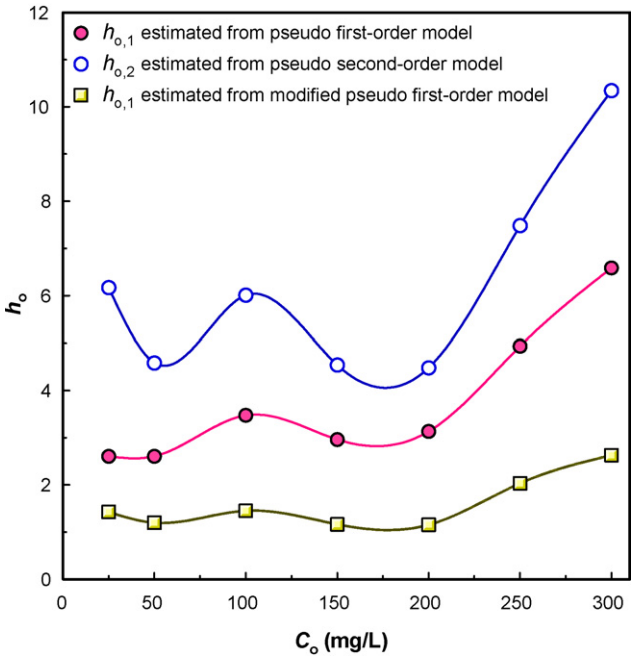

Fig. 6. The variation of the initial rate of adsorption with the initial MB concentration.

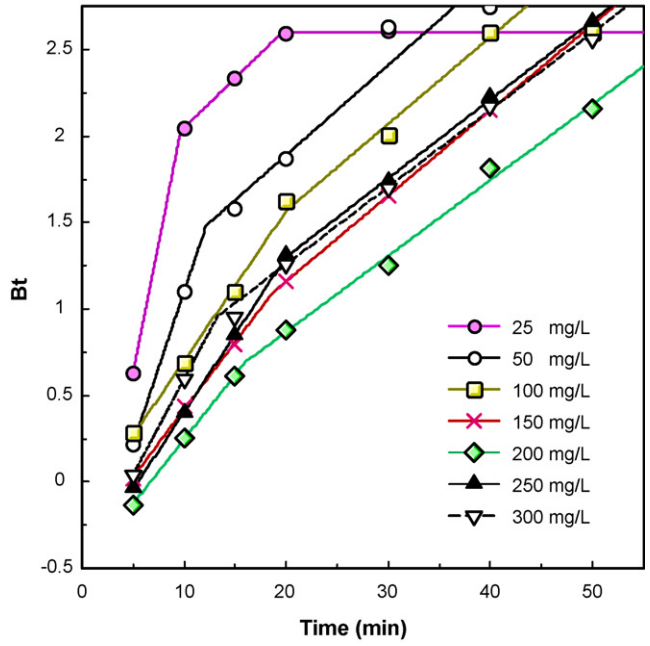

Fig. 7. Boyd plots for MB adsorption on PSH at 30 °C and different initial MB concentrations.

the present time, Boyd's film-diffusion [35] and Webber's pore-diffusion [36] are the two most widely used models for studying the mechanism of adsorption. Both models usually show a multilinear nature in their plots, and the conventional method is that the researcher inspects the plots visually to decide the start and end of each linear segment. In this study, the statistical approach of piecewise linear regression was used to avoid subjective choice of linear segments. The software package NCSS [37] was used to fit the data by the method of piecewise linear regression.

The film diffusion model of Boyd assumes that the main resistance to diffusion is in the thin film (boundary layer) that surrounds the adsorbent particle, this model is expressed as

$$F = 1 - \left(\frac{6}{\pi^2}\right)\exp(-Bt) \tag{16}$$

Where F is the fractional attainment of equilibrium, at different times, t, and Bt is a function of F.

$$F = \frac{q_t}{q_e} \tag{17}$$

where q_t and q_e are the dye uptake (mg/g) at time t and at equilibrium, respectively.

Eq. (16) can be rearranged to

$$Bt = -0.4977 - \ln(1 - F) \tag{18}$$

According to Eq. (18), if film-diffusion controls the overall rate of adsorption, it follows that a plot of Bt versus t must give a straight line whose intercept is −0.4977 and the slope, B, is used to calculate the effective diffusion coefficient, D_i, (cm^2/s) from the equation:

$$B = \frac{(\pi^2 D_i)}{r^2} \tag{19}$$

where r is the radius of the adsorbent particle assuming spherical shape.

Fig. 7 shows the Boyd plots for the first 50 min of MB adsorption on PSH at 30 °C. The plots are linear in the initial period of adsorption and their intercepts are all close to −0.498, indicating that external mass transfer is the rate limiting process in the beginning of adsorption. It is noticed in the figure that during the first 50 min, the values of Bt (which is a function of fractional attainment of equilibrium) decrease as C_0 increases from 25 to 200 mg/L, but above 200 mg/L Bt values become smaller with increasing concentration. This corroborates the trend previously observed of changing k_1 and k_2 with the MB concentration. Table 3 shows the estimated values of D_i, and also the length of the time period of film-diffusion control. At first glance, the duration of film diffusion control seems to fluctuate meaninglessly, but by observing the dye uptake at the end of film diffusion, q_{fd} (mg/g), an explanation can be found. Fig. 8 shows the relationship between the concentration of MB in aqueous solution when film diffusion control ends, C_{fd}, against q_{fd}, the dye uptake at this time. It is seen from the figure that the relationship between C_{fd} and q_{fd} is in agreement with the shape of the multilayer adsorption isotherm of MB on PSH. It is also noticed that the dye uptake corresponding to saturation of the outer surface, q_{fd}, increases steadily with increasing C_0. Therefore, it can be concluded that film-diffusion control ends when the outer surface of PSH is saturated with MB.

On the other hand, Webber's pore-diffusion model was derived from Fick's second law of diffusion [33,36]. This model assumes that:

(i) the external resistance to mass transfer is only significant for a very short period at the beginning of diffusion;
(ii) the direction of diffusion is radial and the concentration;

Table 3
Diffusion coefficients for adsorption of MB on PSH at 30 °C and different initial concentrations (C_0: mg/L; D_i: cm^2/s, q_{fd}: *mg/g*; k_i: mg/g $min^{0.5}$; q_{pd}: mg/g; diffusion period: min)

C_0	$D_i \times 10^6$	q_{fd}	Film diffusion period[a]	$k_{i,1}$	$k_{i,2}$	First pore diffusion period[b]	q_{pd}	Second pore diffusion period[c]
25	48.08	9.72	<10.0	0.115	0.0142	10.4–20.0	9.86	20.0–81.0
50	25.42	14.87	<12.4	0.924	0.272	11.0–28.2	15.05	28.2–60.8
100	13.69	23.68	<23.5	1.009	0.285	18.9–40.0	23.11	>40.0
150	10.78	26.02	<18.6	2.408	1.904	17.0–29.7	25.32	29.7–56.0
200	10.66	29.86	<15.9	5.619	2.837	12.9–22.7	27.63	22.7–62.1
250	12.90	45.75	<20.0	8.801	2.181	13.3–21.4	37.03	21.4–56.5
300	15.65	46.10	<12.2	6.598	2.568	11.1–23.3	45.28	23.3–59.0

[a] Estimated from the end of the first linear segment in the Boyd plot.
[b] Estimated from the beginning of the second linear segment in the pore-diffusion plot.
[c] Estimated from the beginning of the third linear segment in the pore-diffusion plot.

(iii) the pore diffusivity is constant and does not change with time.

The pore diffusion parameter, k_i (mg/g $min^{0.5}$) is defined by

$$q = k_i t^{0.5} \tag{20}$$

where q is the amount adsorbed (mg/g) at time t.

It can be seen from Eq. (20) that if pore-diffusion is the rate limiting step, then a plot of q against $t^{0.5}$ must give a straight line with a slope that equals k_i and an intercept equal to zero.

Fig. 9 shows the pore diffusion plot of MB adsorption on PSH at 30 °C. It is clear that the plots are multilinear, containing four segments. The piecewise linear regression results are presented in Table 3. For all the multilinear plots in Fig. 9, the regression estimates of the first linear segments has intercept values significantly different from zero, suggesting that pore diffusion does not control the overall rate of adsorption at this early stage. Therefore, it is confirmed that the first linear segment represents film-diffusion, and that the second and third linear segments represent two pore-diffusion regimes. The presence of two pore diffusion periods allows the estimation of two pore diffusion parameters, $k_{i,1}$ and $k_{i,2}$ that are presented in Table 3. The rate parameters $k_{i,1}$ and $k_{i,2}$ represent the diffusion in of MG in pores that have two distinct sizes (macropores and mesopores) [38]. Therefore, the decrease in values of k_i for macro- to mesopore diffusion is a direct consequence of the relative free path for diffusion available. As pore size decreases, the path available for diffusion becomes smaller, which leads to a decrease in the rate of diffusion.

It is also observed in Table 3 that an increase in the initial MB concentration increases the pore diffusion rate parameters. This is due to the increase in the bulk liquid dye concentration which increases the driving force for dye diffusion. For each initial concentration of MB, the end of the first linear segment represents the transition from film-diffusion-control to pore-diffusion-control. The dye uptake at this time, q_{pd}, is plotted against the concentration of MB in aqueous solution in Fig. 8, and it is seen from the plot that q_{pd} follows a trend similar to the multilayer adsorption isotherm. The discrepancy near the end of the plot between values obtained from film and pore diffusion-models is due to the few experimental points in the film-diffusion period, which results in uncertainty in predicting the end of the first linear segment for $C_0 = 250$ mg/L.

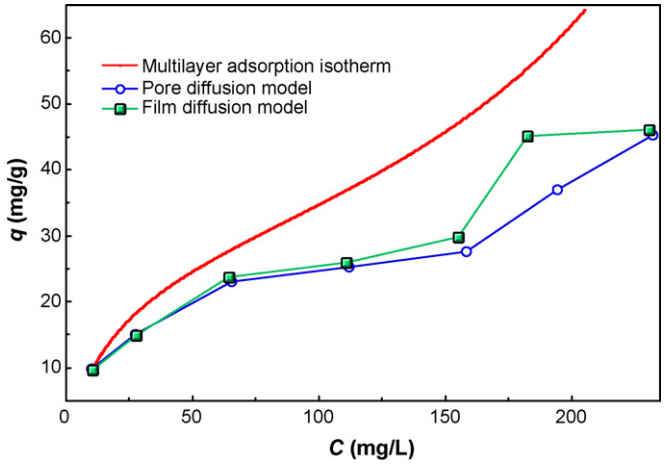

Fig. 8. The relationship between the dye uptake at the time of ending the film diffusion period and the aqueous MB concentration at this time.

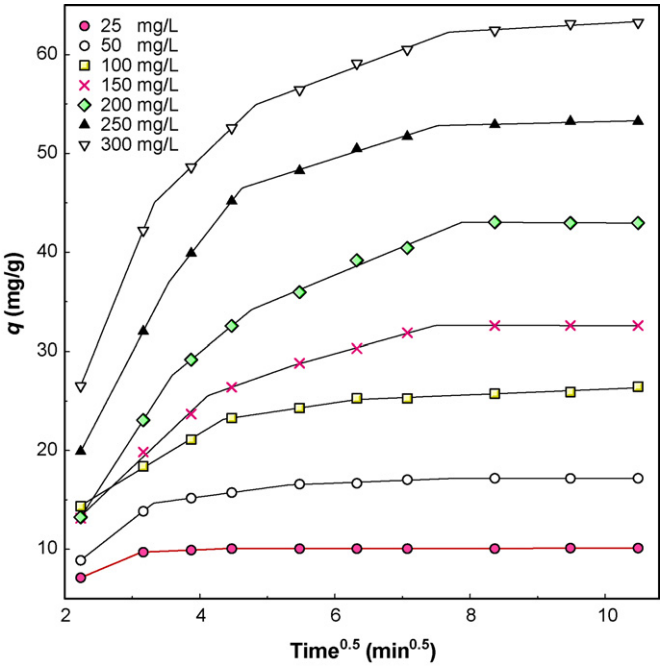

Fig. 9. Intraparticle diffusion plot for the adsorption at 30 °C and different initial MB concentrations.

4. Conclusions

The present study shows that PSH can be used as an adsorbent for the removal of methylene blue dye from aqueous solutions. The amount of dye adsorbed was found to vary with the initial methylene blue concentration and contact time. The multilayer adsorption isotherm was found to have the best fit to the experimental data, suggesting multilayer adsorption on a homogenous surface. The adsorption kinetics can be predicted by both the pseudo-first-order and the modified pseudo-first-order models, while the pseudo-second-order model is applicable at concentrations higher than 50 mg/L. The overall rate of dye uptake was found to be controlled by film diffusion at the beginning of adsorption. As the adsorption time increases, it was found that pore-diffusion becomes the rate controlling step. The multilinearity of pore diffusion plots indicate that there are two distinct pore-diffusion regimes, corresponding to diffusion in macro and mesopores.

Acknowledgments

The authors acknowledge the research grant provided by the Universiti Sains Malaysia under the Research University (RU) Scheme (Project No: 1001/PJKIMIA/814005). The authors thank Ms. I.A.W. Tan for her assistance in FTIR analysis.

References

[1] N. Sapari, Treatment and reuse of textile wastewater by overland flow, Desalination 106 (1996) 179–182.
[2] J.R. Easton, B.D. Waters, J.H. Churchley, J. Harrison, in: P. Cooper (Ed.), Colour in Dyehouse Effluent, Society of Dyers and Colourists, The Alden Press, Oxford, 1995, p. 9.
[3] B.H. Hameed, A.T.M. Din, A.L. Ahmad, Adsorption of methylene blue onto bamboo-based activated carbon: kinetics and equilibrium studies, J. Hazard. Mater. 141 (2007) 819–825.
[4] I.A.W. Tan, B.H. Hameed, A.L. Ahmad, Equilibrium and kinetic studies on basic dye adsorption by oil palm fibre activated carbon, Chem. Eng. J. 127 (2007) 111–119.
[5] B.H. Hameed, A.L. Ahmad, K.N.A. Latiff, Adsorption of basic dye (methylene blue) onto activated carbon prepared from rattan sawdust, Dyes Pigments 75 (2007) 143–149.
[6] I A.W. Tan, A.L., Ahmad, B.H. Hameed, Optimization of preparation conditions for activated carbons from coconut husk using response surface methodology, Chem. Eng. J. (2007), doi:10.1016/j.cej.2007.04.031.
[7] A.A. Ahmad, B.H. Hameed, N. Aziz, Adsorption of direct dye on palm ash: kinetic and equilibrium modeling, J. Hazard. Mater. 141 (2007) 70–76.
[8] M. Hasan, A.L. Ahmad, B.H. Hameed, Adsorption of reactive dye onto cross-linked chitosan/oil palm ash composite beads, Chem. Eng. J. doi:10.1016/j.cej.2007.03.038.
[9] Z. AL-Qoda, Adsorption of dyes using shale oil ash, Water Res. 34 (2000) 4295–4303.
[10] M.C. Ncibi, B. Mahjoub, M. Seffen, Kinetic and equilibrium studies of methylene blue biosorption by *Posidonia oceanica* (L.) fibres, J. Hazard. Mater. B139 (2007) 280–285.
[11] M.I. El-Khaiary, Kinetics and mechanism of adsorption of methylene blue from aqueous solution by nitric-acid treated water-hyacinth, J. Hazard. Mater. 147 (2007) 28–36.
[12] B.H. Hameed, D.K. Mahmoud, A.L. Ahmad, Sorption of basic dye from aqueous solution by pomelo (*Citrus grandis*) peel in a batch system, Colloids Surf. A: Physicochem. Eng. Aspects, doi:10.1016/j.colsurfa.2007.08.033.
[13] A. Mittal, A. Malviya, D. Kaur, J. Mittal, L. Kurup, Studies on the adsorption kinetics and isotherms for the removal and recovery of methyl orange from wastewaters using waste materials, J. Hazard. Mater. 148 (2007) 229–240.
[14] J.F. Osma, V. Saravia, J.L. Toca-Herrera, S.R. Couto, Sunflower seed shells: a novel and effective low-cost adsorbent for the removal of the diazo dye reactive black 5 from aqueous solutions, J. Hazard. Mater. 147 (2007) 900–905.
[15] R. Jain, S. Sikarwar, Removal of hazardous dye congored from waste material, J. Hazard. Mater. (2007), doi:10.1016/j.jhazmat.2007.07.070.
[16] F. Çiçek, D. Özer, A. Özer, A. Özer, Low cost removal of reactive dyes using wheat bran, J. Hazard. Mater. 146 (2007) 408–416.
[17] V. Ponnusami, S. Vikram, S.N. Srivastava, Guava, (*Psidium guajava*) leaf powder: novel adsorbent for removal of methylene blue from aqueous solutions, J. Hazard. Mater. (2007) doi:10.1016/j.jhazmat.2007.06.107.
[18] F. Doulati Ardejani, Kh. Badii, N. Yousefi Limaee, S.Z. Shafaei, A.R. Mirhabibi, Adsorption of Direct Red 80 dye from aqueous solution onto almond shells: effect of pH, initial concentration and shell type, J. Hazard. Mater. (2007) doi:10.1016/j.jhazmat.2007.06.048.
[19] H.D. Grosch, W. Belitz, Food Chemistry, Springer-Verlag, Berlin, 1987.
[20] G.F. Trease, W.C. Vans, Trease and Evans Pharmacognosy, 13th ed., Baillier Tindall, London, 1983, 203.
[21] Y. Bulut, H. Aydın, A kinetics and thermodynamics study of methylene blue adsorption on wheat shells, Desalination 194 (2006) 259–267.
[22] R. Han, W. Zou, W. Yu, S. Cheng, Y. Wang, J. Shi, Biosorption of methylene blue from aqueous solution by fallen phoenix tree's leaves, J. Hazard. Mater. 141 (2007) 156–162.
[23] S. Cengiz, L. Cavas, Removal of methylene blue by invasive marine seaweed: *Caulerpa racemosa* var. *cylindracea*, Bioresour. Technol. (2007) doi:10.1016/j.biortech.2007.05.011.
[24] H.M.F. Freundlich, Uber die adsorption in Losungen, Z. Phys. Chem. 57 (1906) 385–470.
[25] I. Langmuir, Constitution and Fundamental Properties of Solids and Liquids, I. Solids, J. Am. Chem. Soc. 38 (11) (1916) 2221–2295.
[26] J. Wang, C.P. Huang, H.E. Allen, D.K. Cha, D.W. Kim, Adsorption characteristics of dye onto sludge particulates, J. Colloid Interface Sci. 208 (1998) 518–528.
[27] R.A. Shelden, W.R. Caseri, U.W. Suter, Ion exchange on muscovite mica with ultrahigh specific surface area, J. Colloid Interface Sci. 157 (2) (1993) 318–327.
[28] C.H. Weng, Adsorption characteristics of new coccine dye on to sludge ash, Adsorp. Sci. Technol. 20 (7) (2002) 669–681.
[29] C. Kaewprasit, E. Hequet, N. Abidi, J.P. Gourlot, Application of methylene blue adsorption to cotton fiber specific surface area measurement: Part I. Methodology, J. Cotton Sci. 2 (1998) 164–173.
[30] C.H. Giles, R.B. McKay, Adsorption of cationic (basic) dyes by fixed yeast cells, J. Bacteriol. 89 (2) (1965) 390–397.
[31] S. Lagergren, Zur theorie der sogenannten adsorption geloster stoffe, Kungliga Svenska Vetenskapsakademiens, Handlingar 24 (4) (1898) 1–39.
[32] Y.S. Ho, Adsorption of heavy metals from waste streams by peat, Ph.D. Thesis, University of Birmingham, Birmingham, U.K., 1995.
[33] X. Yang, B. Al-Duri, Kinetic modeling of liquid-phase adsorption of reactive dyes on activated carbon, J Colloid Interface Sci. 287 (1) (2005) 25–34.
[34] M. Badertscher, E. Pretsch, Bad results from good data, Trends Anal. Chem. 25 (2006) 1131–1138.
[35] G.E. Boyd, A.W. Adamson, L.S. Myers Jr., The exchange adsorption of ions from aqueous solutions by organic zeolites, II: kinetics, J. Am. Chem. Soc. 69 (1947) 2836–2848.
[36] W.J. Weber Jr., J.C. Morris, Kinetics of adsorption on carbon from solution, J. Sanit. Eng. Div. Proc. Am. Soc. Civil Eng. 89 (1963) 31–59.
[37] J. Hintze, NCSS, PASS, and GESS, NCSS, Kaysville, Utah, 2006.
[38] S.J. Allen, G. McKay, K.Y.H. Khader, Intraparticle diffusion of a basic dye during adsorption onto sphagnum peat, Environ. Pollut. 56 (1989) 39–50.